

# The Array Network Facility Seismic Bulletin: Products and an Unbiased View of United States Seismicity

by **Luciana Astiz, Jennifer A. Eakins, Vladislav G. Martynov, Trilby A. Cox, Jonathan Tytell, Juan C. Reyes, Robert L. Newman, Gulsum H. Karasu, Taimi Mulder, Malcolm White, Geoffrey A. Davis, Robert W. Busby, Katrin Hafner, Jon C. Meyer, and Frank L. Vernon**

*Online Material:* Movies of temporal deployment of USArray and seismicity: event processing flow chart; travel-time and magnitude statistics plots; tables of earthquake catalogs, magnitude bias, and picked arrivals.

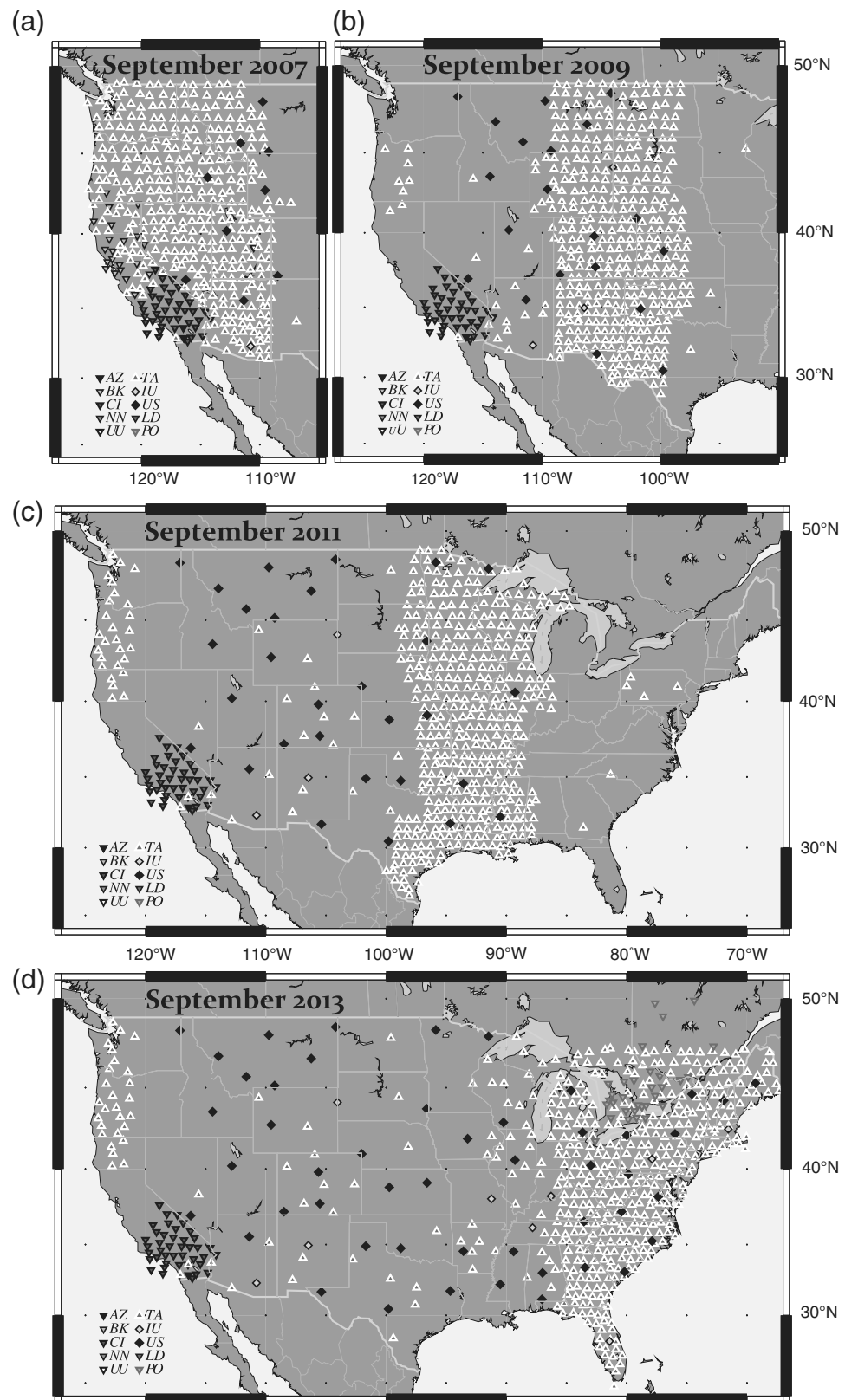
## INTRODUCTION

The Array Network Facility (ANF), funded by the National Science Foundation Earthscope-USArray project, is responsible for (1) collection of all transportable array (TA) station data and generation of station metadata; (2) their delivery to the Incorporated Research Institutions for Seismology Data Management Center (IRIS-DMC). (3) Providing useful interfaces for field operations personnel at the Array Operations Facility (AOF) to obtain state-of-health information; (4) TA station command and control, such as seismometer mass centering and calibration; (5) collection of data from contributing regional network stations; and (6) data quality monitoring and control. Herein, we provide a brief overview of the evolution of USArray operations with emphasis on aspects relevant to the production of the ANF Seismic Bulletin.

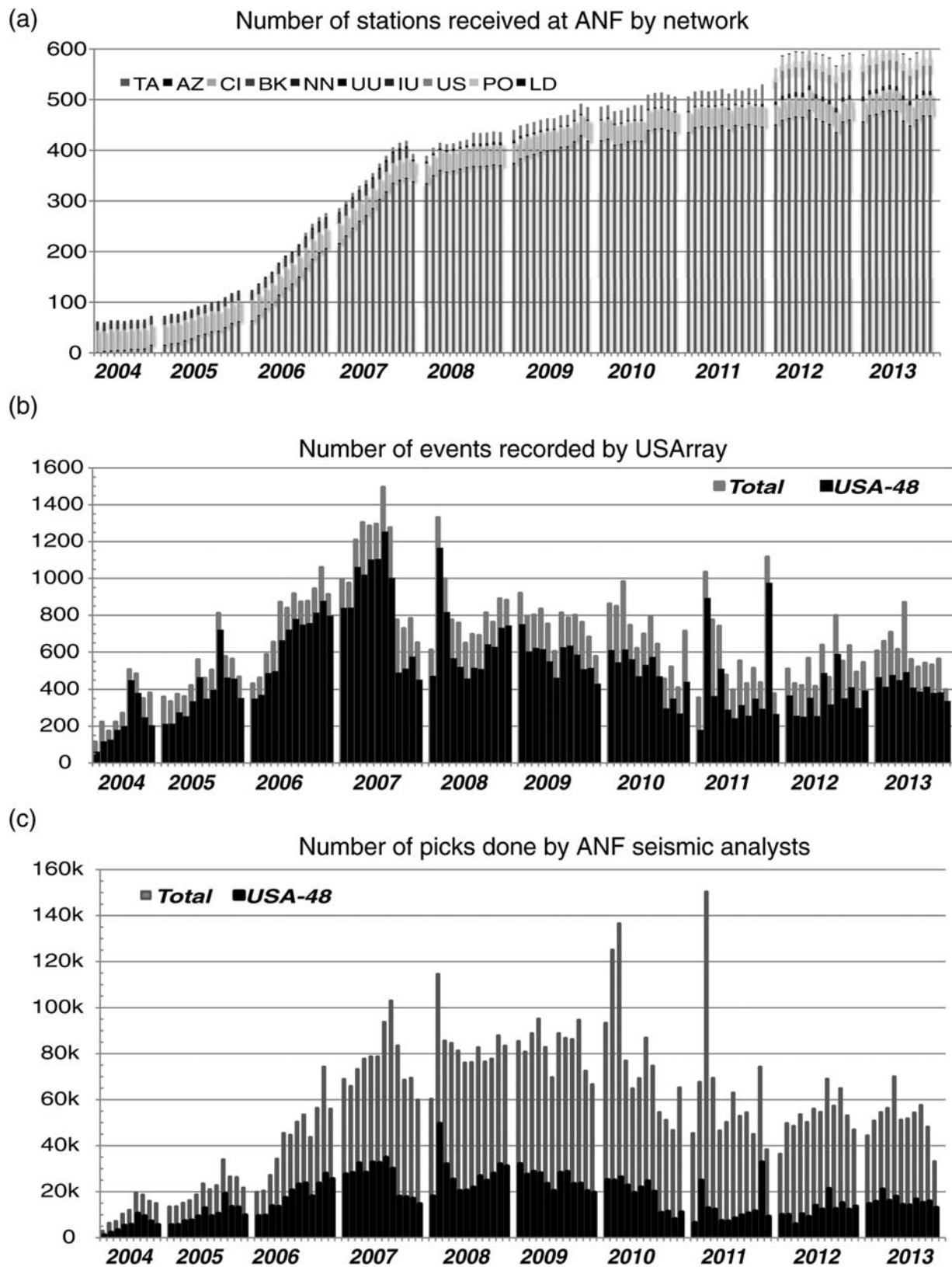
To begin operations at the ANF, real-time acquisition of continuous three-component broadband seismic data from 62 regional stations in California was initiated in April 2004. Seismic and state-of-health data from TA stations started flowing to the ANF shortly thereafter, with 73 stations transmitting data continuously by the end of 2004. A steady influx of data from newly deployed TA stations ensued with the first footprint of 400 USArray stations operating by mid-September 2007 (Figs. 1a and 2a). USArray then began to migrate or roll eastward at an annual rate of about 200 stations, with the second and third distinct footprints being deployed by September 2009 and 2011, respectively (Fig. 1b and c). Deployment of the last distinct footprint was completed by October 2013. Figure 1d shows USArray stations locations as of September 2013.

The monthly tally of contributing and TA stations by network between April 2004 and November 2013 has steadily increased (Fig. 2a). Each of the approximately 500 TA stations transmits: 6 seismic (three BH? channels recording at 40 samples/s and three LH? channels at 1 sample/s) in real time. Longer period seismic channels (VH? and UH? recording 1 sample every 10 and 100 s, respectively) are retrieved routinely from station balers by ANF and sent to the DMC. The overall daily data availability of real-time data to date is 94% when weighted by the number of stations, with the median daily data return being 98%, well over the 85% operational goal set for this project. Deployment of infrasound sensors at TA stations started in October 2010. During the last 10 years, TA stations have been deployed at 1691 sites with regional and national (United States and Canada) seismic network operators contributing data from 156 existing stations to USArray. The four-letter station codes of TA stations suggest the grid pattern. The first letter indicates the north/south latitude location with (A–Z, 1–9, and 0). The two middle characters are 2 digit numbers that increase eastward with the last character being usually ‘A.’ The exceptions are California station codes that end in ‘C,’ and stations that have been relocated near the original site, which end in ‘B’; the last character for stations located south of 26.5° is ‘Z’ so that station codes are unique. Movies of the monthly deployment maps of the seismic network are available at [http://anf.ucsd.edu/stations/deployment\\_history.php](http://anf.ucsd.edu/stations/deployment_history.php) (last accessed March 2014). The rolling and cumulative deployment movies until November 2013 can be found in Movies S1 and S2, respectively, available in the electronic supplement to this article.

Seismic network operators observe that data quality improves when seismic analysts pick seismic phases and locate events routinely. This observational approach to monitoring data quality has been used at the ANF since the start of the USArray deployment. ANF analysts pick mostly primary phases (*P* and *S*) of all recorded events at USArray stations and locate those events



▲ **Figure 1.** Maps showing the location of USArray stations during the (a) first, (b) second, (c) third, and (d) fourth distinct footprints deployed by September 2007, 2009, 2011, and 2013, respectively. The legend indicates the corresponding network symbols and codes for the regional contributing seismic stations, as well as TA, Global Seismographic Network, and backbone stations. Individual monthly deployment maps and tables of USArray stations can be found at [http://anf.ucsd.edu/stations/deployment\\_history.php](http://anf.ucsd.edu/stations/deployment_history.php) (last accessed March 2014).



▲ **Figure 2.** (a) Number of stations received at the ANF by network each month. Network code names can be found at <http://www.iris.edu/dms/nodes/dmc/services/network-codes/> (last accessed March 2014). (b) Number of events recorded by USArray per month. Light gray bars show the total number of events analyzed at ANF, with the overlying black correspond to the number of events located within the conterminous United States. (c) Number of picks made by ANF analysts. Light gray bars represent the number of arrivals per month, whereas the black bars correspond to those from events located within the continental United States.

occurring within the USArray footprint. For example, large location residuals at newly installed stations of ongoing seismicity allow identification of station location errors in the station metadata. Reporting noisy or flat recordings at a particular station allows for prompt investigation and reporting to AOF field engineers or regional network operators for timely resolution.

As of 30 November 2013, ANF seismic analysts have picked over 6.7 million arrivals from about 78,057 events. Over 4.6 million arrivals generated by teleseismic events have been associated with the United States Geological Survey (USGS) earthquake bulletin distributed by the National Earthquake Information Center (NEIC) (<http://earthquake.usgs.gov/regional/neic/>) (last accessed March 2014). The number of events and active stations increase until mid-2007, when the first USArray footprint was deployed (Fig. 1a). The sharp decrease in the number of events at that time corresponds to an operational change at ANF. The automatic processing system triggered an event location from detections at five stations within 200 km until mid-August 2007 when the minimum number of stations required trigger a location was increased to 10. In April 2012, this parameter was decreased to seven to locate smaller events in the eastern part of the country. In regions at which TA stations have been deployed, USArray data is being mined for microseismicity such as in Arizona (Lockridge *et al.*, 2012) and Oklahoma (Holland *et al.*, 2012). Although 73% of the events recorded by USArray stations are located within the continental United States (black bars in Fig. 2b), the majority (~70%) of ANF picks are generated by global seismicity as most USArray stations record teleseismic events (gray bars in Fig. 2c). Figure 2 presents a compressed view of the data flow into the ANF, number of USArray stations, and the outflow of ANF products (events reported and picked). Burdick *et al.* (2008, 2009, 2010, 2012, 2013) have used teleseismic ANF Bulletin *P*-phase arrivals to construct increasingly refined tomographic images under the continental United States. Although ANF Bulletin *Pn*-phase arrivals have been used by Buehler and Shearer (2010) to define the shallower structure under the western United States.

**Building of the ANF Seismic Bulletin and Overall Characteristics** section describes the ANF Seismic Bulletin, focusing on the procedures used to locate events within the footprint of the USArray. It also associates teleseismic arrivals with both the Quick Epicenter Determination (QED) and QED weekly seismic catalogs produced by the United States Geological Survey at the National Earthquake Information Center (USGS-NEIC) (<http://earthquake.usgs.gov/data/pde.php>) (last accessed March 2014).

**Global Seismicity Observed with the USArray** section focuses on events recorded at teleseismic distances and shows maps of global seismicity and the temporal distribution of that seismicity. We present travel-time plots of associated analyst picks of USArray stations data received at ANF between April 2004 and November 2013 for both teleseismic and regional events.

**Observed Seismicity of the Continental United States** section presents overall seismicity within the continental United States between April 2004 and November 2013, including the distribution of events reported by the ANF Seismic

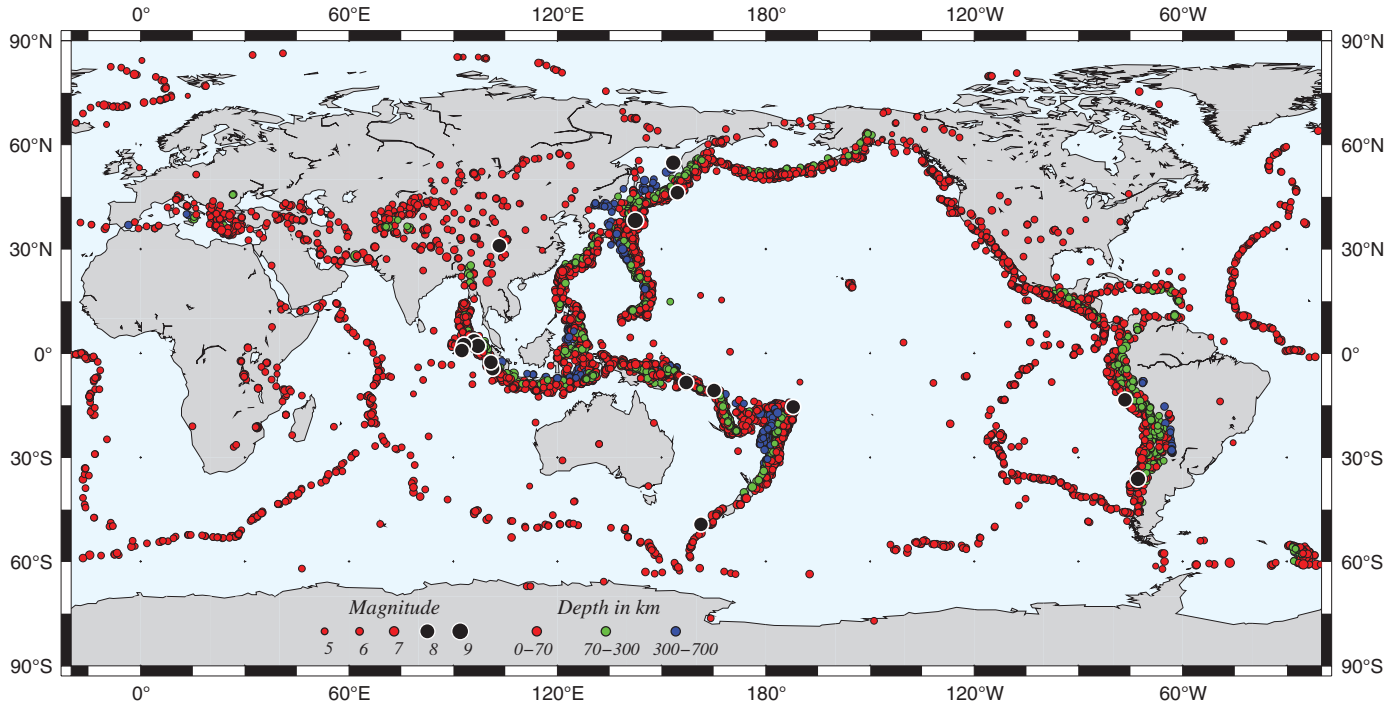
Bulletin only. The temporal and spatial distribution of U.S. seismicity using ANF event locations is explored to assess whether these events are natural or anthropogenic in origin. For most ANF determined hypocenters, Richter local magnitude has been calculated using stations within 600 km as defined by Richter (1958), and referred to as  $M_R$  by Kanamori (1983). We include comparisons of  $M_R$  determined at ANF with magnitudes determined by regional seismic network operators and try to assess if differences for different regions may be associated with different tectonic regimes.

## BUILDING OF THE ANF SEISMIC BULLETIN AND OVERALL CHARACTERISTICS

The ANF uses the Antelope environmental monitoring software package developed by Boulder Real-time Technologies (BRTT) to process and monitor most of the operational tasks for data collection and transfer (<http://www.brtt.com/>; last accessed March 2014). Given the dynamic nature of the USArray, with about 20 stations migrating monthly, the travel-time grids needed for event location and metadata are updated approximately twice per week at ANF. The frequently updated metadata are available at the DMC and through the ANF website (<http://anf.ucsd.edu/tools/dataless/>; last accessed March 2014).

Event data processing flow of the three-component broadband seismic data through the ANF Antelope follows in this paragraph. ① A data flow chart is found in Figure S1. Most automatic processes take place concurrently and continuously such as the real-time data acquisition and processing, and the automatic collection of external bulletin solutions (e.g. the initial QED seismic bulletin and other regional seismic catalogs). Hereafter, Antelope commands will be indicated in *italics*. At TA stations data is recorded by Quanterra Q330 digitizers and stored locally on Quanterra balers. All data are acquired using *q3302orb* from TA stations to the ANF acquisition system in which data are written to an orb server. Then, using *orb2orb* the waveform data are written into the ANF operational system, in which all data processing takes place. The seismic data are parsed through a series of automatic detectors (*orbdetect*). *P*-wave detections are made using vertical channel data, whereas horizontal channels are used for *S*-wave detections. The detections are accumulated and processed through *orbassoc*, which attempts to associate detections over a 500 s time window with teleseismic, regional, and local travel-time grids to determine if the minimum number of arrivals (*na*) that may be associated within a certain distance, which has been set to 200 km to minimize false event triggers. In the event of a false trigger, analysts delete the spurious arrivals and corresponding events, which account for less than 0.01% of events in the automatic system. Further associations are made with the initial automatic QED solutions acquired using *bulletin2orb* against the automatic event associations. The automatically determined local hypocenters are also associated with regional seismic bulletins. The value of *na* changed from 5 to 10 on 16 August 2007 and then to 7 on 1 April 2012. The location algorithm uses the IASP91 velocity model (Kennett, 1991; Kennett and Engdahl, 1991) for all automatic and analyst reviewed locations.

12,221 events with  $M \geq 5.0$  recorded by USArray from April 2004 to November 2013



▲ **Figure 3.** Seismicity as recorded by USArray between April 2004 and November 2013. During this time 12,221 events with  $M \geq 5.0$  produced about 2.6 million associated arrivals in the ANF Seismic Bulletin. Event magnitude is shown by the circle size with color denoting event depth. Black circles show the location of the 15 great  $M \geq 8.0$  shallow earthquakes and the May 2013 deep Kurile event (© Table S1).

Once an automatic event solution exists, ANF analysts use ***dbloc2***, which is based on ***locsat*** of Bratt and Bache (1988) and/or ***genloc*** (Pavlis *et al.*, 2004) to refine the automatic picks and improve the event location. ANF analyst aim to pick *P* waves on vertical component unfiltered waveforms, and *S* waves on one of the horizontal components. If this is not possible, then a 1 s high-pass filter is used for local events and a narrow bandpass filter (0.8–3 Hz) on teleseismic arrivals. Richter (1958, pp. 340–344) magnitudes  $M_R$  are calculated automatically after the first analyst review for all events located within the local grid. Because external seismic catalogs are updated continuously, ANF analysts reassociate each event with the updated catalogs about one week after the initial location and assign an authoritative hypocentral solution. If an event occurs within the domain of a particular regional seismic network the location of that network, when available, is deemed the preferred origin.

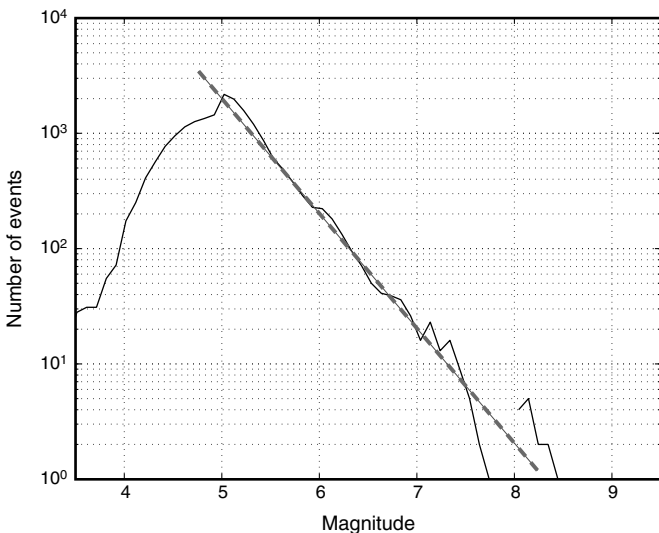
Archived monthly databases are created from the real-time database. The final analyst review takes place using these databases. The objective of the final review is to ensure that events with NEIC  $M \geq 5.0$  have not been missed by prior processing, arrivals from stations, which may not have been available in prior reviews are picked and associated, and all arrivals are associated with a single event, and authoritative locations are designated as preferred origins. By the time the final review takes place, associations are made with final locations from regional networks and the USGS ([earthquake.usgs.gov/data/pde.php](http://earthquake.usgs.gov/data/pde.php); last accessed March 2014). Finally, missing  $M_R$  magnitudes are calculated for events occurring within the local grid, and

a final association with external catalogs is carried out to ensure that all available origins are associated with events. Once the final analyst review of a monthly database is complete, the event bulletin is reformatted using ***db2ims*** and ***ims2dmc*** and exported using ***orbxfer2*** to the DMC. The final ANF Seismic Bulletin picks are forwarded to the International Seismological Center (ISC) by the DMC. At the time of this publication, this final process takes place about 3 months behind real time.

The ANF Bulletin, composed of earthquake locations, associated picks, and associated event origins, is available through the web data product interface SPUD at the IRIS-DMC (<http://www.iris.edu/spud/>; last accessed March 2014). The ANF monthly databases, including all origin and arrival data, are also available in CSS3.0 format at <http://anf.ucsd.edu/tools/events/> (last accessed March 2014). Special event pages are generated within 24 h at <http://anf.ucsd.edu/spevents> (last accessed March 2014), for  $M \geq 7.0$  teleseismic events, for regional earthquakes with  $M \geq 5.0$ , or for felt or damaging events with lower magnitudes occurring in the United States. The special event archive is accessible for two years following an event.

## GLOBAL SEISMICITY OBSERVED WITH THE USARRAY

ANF analysts review seismic phases for global events with NEIC  $M \geq 5.0$  recorded at USArray stations. Between April 2004 and November 2013, there have been 12,221 such earthquakes falling on most plate boundaries (Fig. 3). Sixteen



**▲ Figure 4.** Magnitude distribution of the teleseismic events reported in the ANF Seismic Bulletin (Figs. 3 and [S1](#)). The rapid decrease in the number of teleseismic events with decreasing magnitude reflects that ANF analysts strive for completeness of  $M \geq 5.0$  teleseismic events only. The dashed line has a slope of  $-1$ .

$M \geq 8.0$  events have also occurred during this time ([Table S1](#)). Figure 4 shows the magnitude distribution for these events and the teleseismic events with  $M < 5.0$  displayed in [Figure S2](#). USArray stations recorded 8220 earthquakes located mainly around the Pacific Rim, Indonesia, and the North Atlantic Ridge with  $4.0 \leq M < 5.0$  ([Fig. S2a](#)). The distribution of the remaining 228 earthquake locations with  $M < 4.0$  is more scattered ([Fig. S2b](#)); mostly these events occurred in the Caribbean, South America, the Aleutians, the western Pacific (Kuriles, Japan, Marianas, and Tonga), and at some of the midocean ridges. Smaller events that were recorded occurred within the Gulf of California, the Mid-America trench, and offshore Mexico.

There are about 2.4 million phase picks included in the ANF Seismic Bulletin from the events displayed in the map in Figure 3 are plotted in the travel-time graphs (Fig. 5). The number of picks for different seismic phases for  $M \geq 5.0$  events grouped by the USGS depth definitions is listed in [Table S2](#). Picks are color coded with respect to their associated phases in the ANF Bulletin with colors similar to those used in the tenth Anniversary IRIS Poster ([Astiz et al., 1996](#)). For example, compression phase picks are shown with blue hues; those for shear phases are depicted by red and green tones; and those for mixed phases are shown in yellow or violet tones.

Figure 5 shows the arrival picks associated with shallow events (depth  $< 70$  km) occurring between April 2004 and November 2013, which are displayed in Figure 3 by red circles. The histogram in the upper left shows the depth distribution of the PDE hypocenter for these events in 1 km increments. The peaks at depths of 10 and 35 km are from earthquakes with poorly constrained depths, which were manually assigned

by USGS seismologists. The bulk of the arrivals in the bulletin are associated with  $P$ ,  $PKP$ , or  $PKiKP$  phases, because ANF analysts mostly pick first arriving phases ([Table S2](#)). USArray has recorded shallow events at ranges from  $0^\circ$  to  $180^\circ$  during this period. The arrivals from these events are in good agreement with the IASP91 theoretical travel-time curves for a 10 km deep source ([Fig. S3](#)).

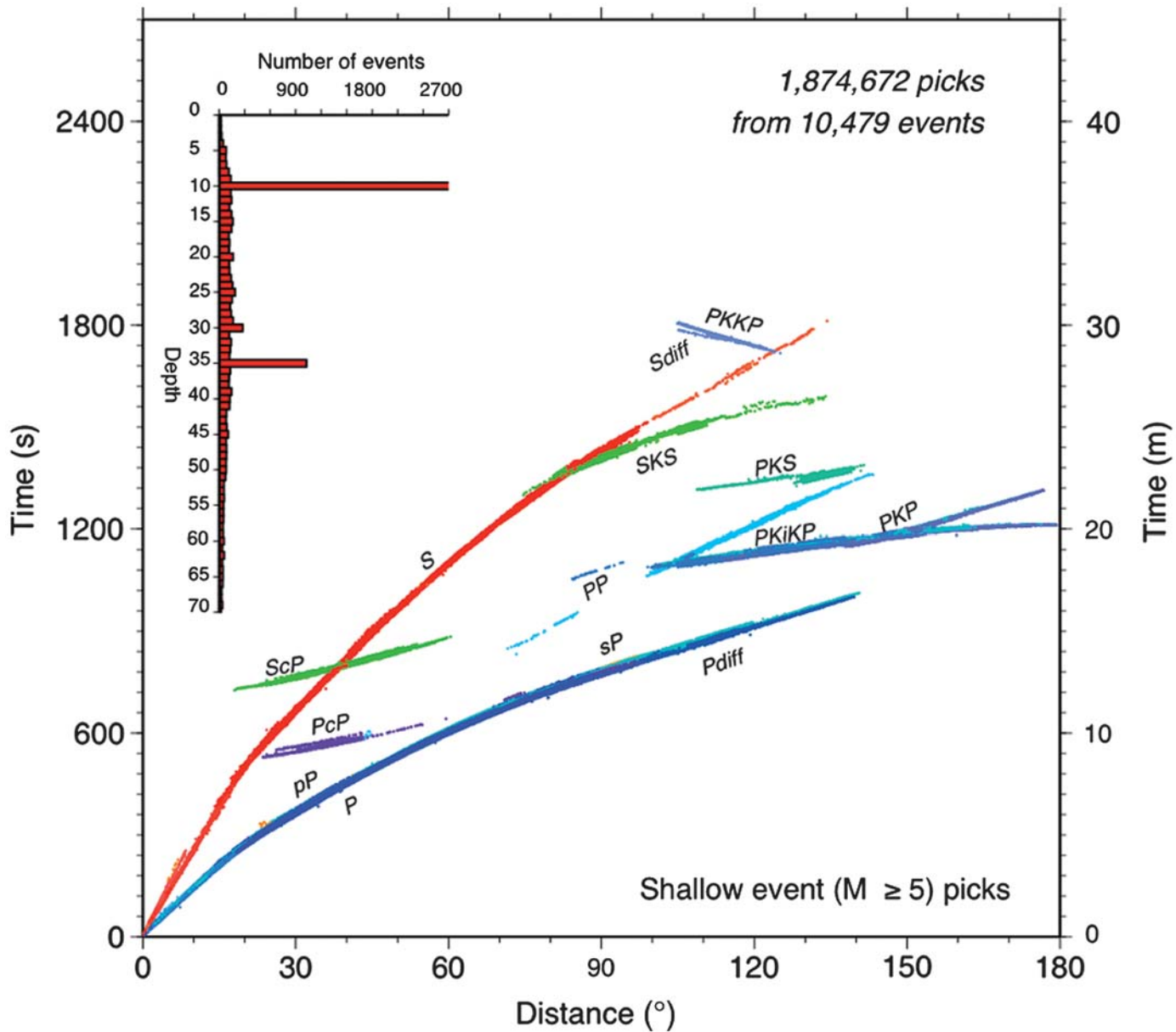
Phase arrivals for intermediate-depth ( $70 \leq \text{depth} < 300$  km) events, that are shown by green circles in Figure 3, comprise about 16% of the teleseismic picks made by ANF analysts are displayed in a travel-time graph in the [Figure S4a](#). The distance range covered by USArray stations for intermediate-depth event arrivals is from about  $10^\circ$ – $160^\circ$ , but it is possible that, as the USArray is deployed along the East Coast, arrivals at larger distances may be reported in the ANF Bulletin. For a given distance and phase, the picks are more spread than those of shallow sources due to the larger span of event depths. Theoretical travel-time curves for a source at 120 km depth for the IASP91 velocity model is shown in [Figure S4b](#), which is in good agreement with the associated phase picks ([Fig. S4a](#)).

Travel-time plots from phase arrivals of deep events ( $300 \leq \text{depth} < 700$  km) are shown in the [Figure S5a](#). These arrivals represent about 5% of the ANF Bulletin picks for the events shown by blue circles in the map in Figure 3. The distance range covered by arrivals of deep events is limited (from about  $40^\circ$  to  $150^\circ$ ). Because deployment of TA stations is complete, and deep events (blue circles in Fig. 3) do not occur as regularly as intermediate-depth events, we expect that the range coverage of these events will remain approximately the same. Arrivals for a particular seismic phase at a given distance are even more diffuse than those of intermediate-depth events due in part to their bimodal depth distribution as well as the larger range of event depths included. IASP91 theoretical travel-time curves for a deep source at 550 km are displayed in the supplement Figure S5b.

Because the Antelope system uses CSS3.0 database tables to record all information regarding not only the metadata but also the results of picking and event location, it is simple to determine which events are associated with particular phases by using commands such as `dbsubset` and `dbjoin`. For example,  $PKP$  arrivals shown in Figure 5 were generated by a few shallow events occurring in the Celebes, New Guinea, South America, and the Hindu Kush region. Those for intermediate-depth and deep events ([in Figs. S4a and S5a, respectively](#)) originate from events in the Philippines, Solomon Islands, and New Guinea. The arrivals for  $P'$  phases ( $PKPPK$ ) for both intermediate-depth and deep events are generated by events occurring in the Kurile Islands and South America.

## OBSERVED SEISMICITY OF THE CONTINENTAL UNITED STATES

ANF locates and associates events recorded by USArray stations for events occurring within the footprint of USArray,



**▲ Figure 5.** Travel-time plot of ANF picks for the shallow events (depth < 70 km) occurred between April 2004 and November 2013, are shown by red circles in Figure 3. Bar plot in the upper left shows the depth distribution of these events with maximum peak at 10 km depth with nearly 2700 events. Different colors indicate different associated phase picks in the ANF Seismic Bulletin. The number of associated phase picks for each seismic phase is listed in [Table S2](#). Theoretical travel times for a 10 km deep source are found in [Figure S3](#).

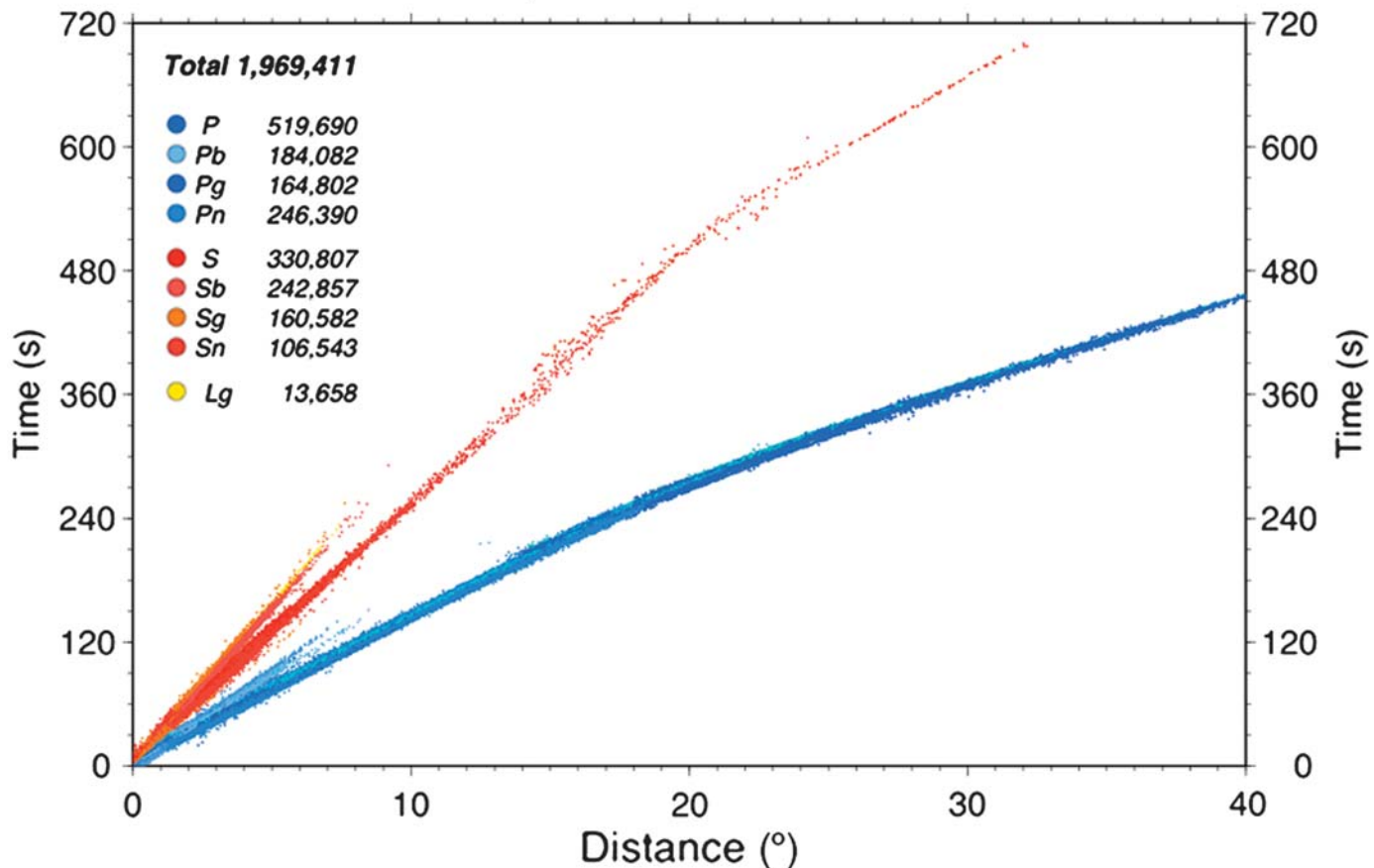
as discussed in [Building of the ANF Seismic Bulletin and Overall Characteristics](#) section. Figure 6 shows the travel-time plot with over 2.0 million crustal phases picked by ANF analysts for 57,606 events occurring between April 2004 and November 2013. Travel times plotted are associated with the preferred origin of the events located within the conterminous United States, as defined by the bounding box in Figure 7. Travel-time plot of arrivals associated with ANF locations for these events shows a similar pattern to that of Figure 6.

Figure 7 shows the events occurring within the region enclosed by the red boundary hereinafter referred to as the con-

tiguous United States. The epicenters plotted correspond to the ANF assigned preferred origin in this figure demonstrates that ANF analysts assign preferred origins to regional bulletin solutions located within or near the delineated authoritative regions (Table 1).

Continental United States seismicity recorded at USArray stations delineates the western plate boundary of North America, the broad zone of deformation to the east of the Basin and Range province, and the eastern boundary of the Snake River Plain and the Rocky Mountains. However, the USArray has been instrumental in highlighting zones of seismicity fur-

Arrivals associated with 57,606 preferred origins of events occurred  
from April 2004 to November 2013



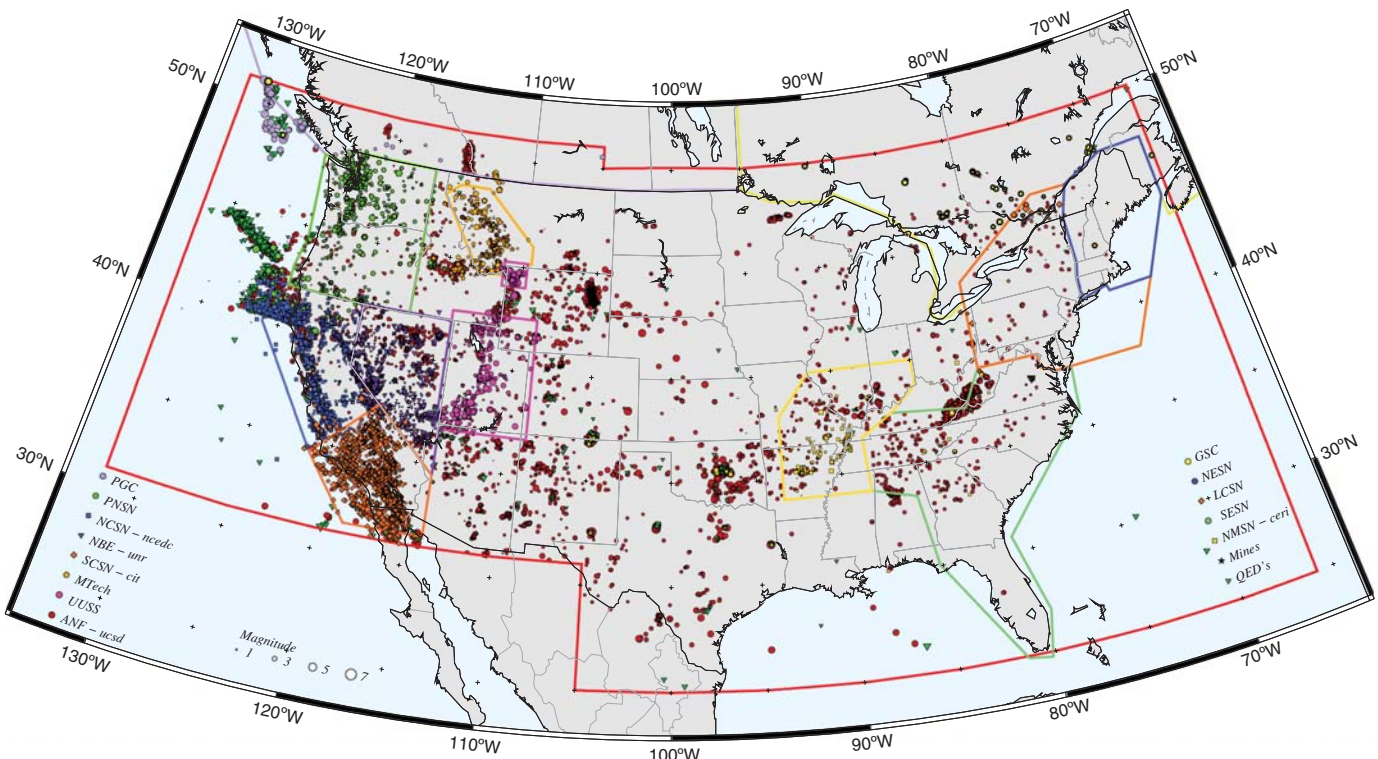
▲ **Figure 6.** Travel-time plot of ANF picks for the preferred origin locations of the events that occurred within the continental U.S. The colors correspond to the phase picks associated in the ANF Seismic Bulletin for each of the picks. The number of associated phase picks is displayed in the top left.

ther east, in the central United States at which regional seismic networks are sparse. TA station data played a crucial role in determining the nature of the event that occurred at the Crandall Canyon mine in central Utah in August 2007 (Pechmann *et al.*, 2008; Ford *et al.*, 2008). More recently, seismic activity in Oklahoma (Holland and Gibson, 2012) and Arkansas has been well recorded by nearby TA stations. Holland *et al.* (2012) have incorporated data from TA stations into the Oklahoma regional seismic network to improve event locations. A fuller discussion of seismic activity in the continental United States by region is beyond the scope of this study.

The ANF Seismic Bulletin contains 53.2% more events than those reported by other networks between April 2004 and November 2013. The six panels in Figure 8 show the location of events reported only by the ANF Bulletin in 18–23 month periods. Table 2 lists the total number of origins in the ANF Seismic Bulletin per calendar year and the number of events reported only by the ANF within the continental United States. This ranges from a few percent whereas the

USArray was deployed only in California up to 80% when the USArray footprint was in the midcontinent.

A comparison of Figures 7 and 8 shows that many of the events having only ANF solutions are located primarily in regions lacking good regional seismic network coverage, such as the midcontinent and offshore northwest regions. However, many events for which there are only reported ANF hypocenters occur within areas monitored by regional network monitoring areas. Regional seismic bulletins generally do not include man-made events such as mining blasts (J. C. Pechmann, personal comm., 2012), whereas the ANF Seismic Bulletin reports all events recorded by USArray stations regardless of their source. ANF analysts may suspect the anthropogenic origin of a particular event due to waveform characteristics such as emergent *P* arrivals or small-amplitude *S* waves. Nevertheless, discrimination of blasts is not carried out, as it would be a considerable operational challenge given the geographical extent and dynamic nature of the USArray. However, we assess here whether these uniquely reported events are



**▲ Figure 7.** Location of 57,606 preferred origins in ANF Seismic Bulletin for each event recorded by USArray stations in the continental U.S. from April 2004 to November 2013. Gray lines show state borders. Colored polygons delineate the ANSS authoritative regions (Table 1) for each regional network indicated. Symbols and colors correspond to the preferred reporting network as indicated in the map legend. Symbol size is proportional to the magnitude of each event.

**Table 1**  
**Organizational Abbreviations**

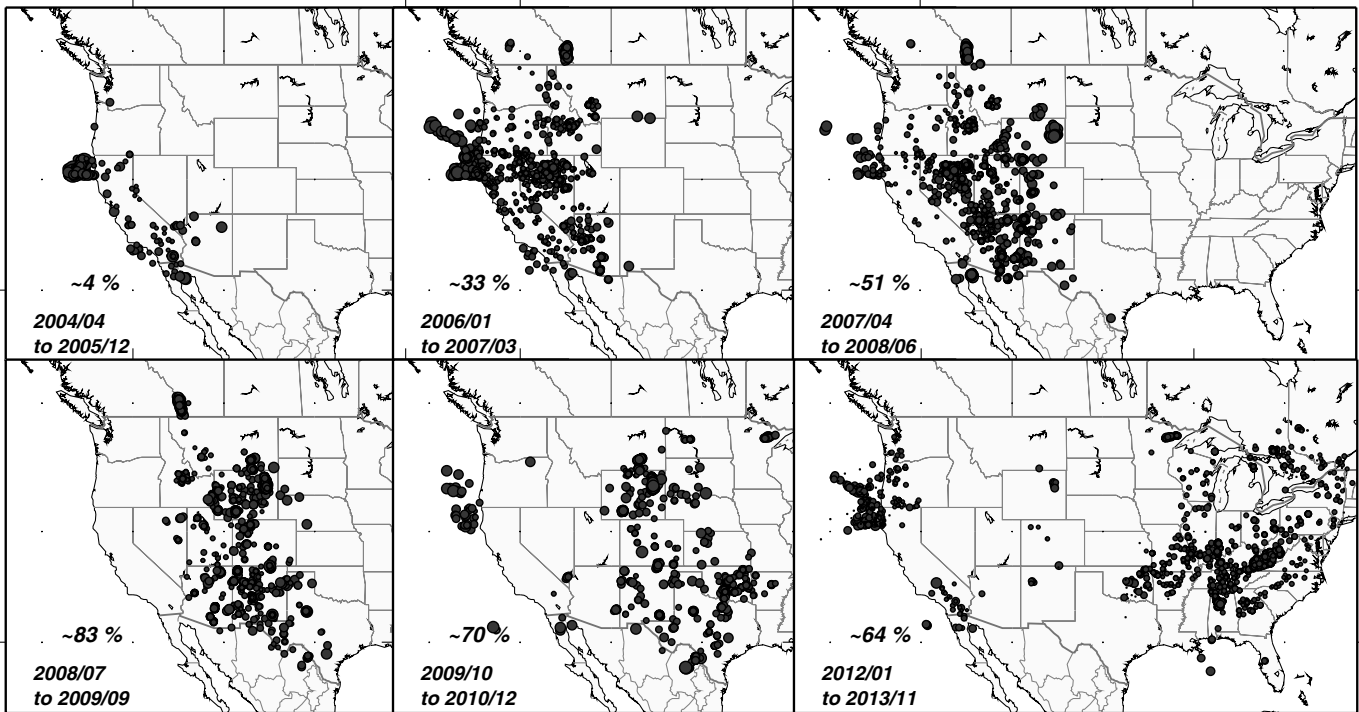
Organization Name	Abbreviation
Advanced National Seismic System	ANSS
National Research Council of Canada	NRCC
Array Network Facility	ANF
Global Seismographic Network	GSN
California Institute of Technology (Caltech)/ Southern California Seismic Network	CIT/SCSN
Nevada Bulletin of Earthquakes/University of Nevada at Reno	NBE/UNR
Northern California Seismic Network/ Northern California Earthquake Data Center	NCSN/NCEDC
Pacific Northwest Seismic Network	PNSN
Pacific Geoscience Center	PGC
Montana Tech of the University of Montana	MTECH
Utah University Seismic Service	UUSS
New Madrid Seismic Network/Center of Earthquake Research Institute	NMSN/CERI
South East Seismic Network	SESN
Lamont-Doherty Columbia Seismic Network	LCSN
New England Seismic Network	NESN
Geological Survey of Canada	GSC

anthropomorphic in origin or an indication that smaller earthquakes are being located due to greater station coverage. Although determining whether events are tectonic, triggered by waves of great earthquakes ([van der Elst et al. 2013](#)) or induced by humans ([Ellsworth, 2013](#)) is a matter of great interest but beyond the scope of this study.

#### A Local-Time View of the ANF Bulletin

On a time scale of years, it seems reasonable to expect that background seismicity for a given tectonic region is random throughout the day. However, mine blasting in the United States is allowed only between sunrise and sunset (Mining Safety and Health Administration, Title 30 CFR, MSHA, U.S. Department of Labor). Thus, an increase in seismic activity during local daylight hours may be due to mining activity as documented in southern California by [Agnew \(1990\)](#). We apportion the seismicity reported in the ANF Bulletin between April 2004 and June 2013 by time zones as they roughly coincide with different tectonic regimes in the continental United States, that is, the more active Pacific and Mountain regions and the less active central and eastern regions. First, we determine for each event the time zone in which a particular event occurred and its corresponding local time, while taking into account daylight savings time changes as well as the day of the week. Then we assume that all events within a region occurred within a 24 h period (a virtual day) for each time zone

**Percentage of Events reported only by the ANF Seismic Bulletin**



▲ **Figure 8.** Locations of events reported only in the ANF Seismic Bulletin, ~53% of all events between April 2004 and November 2013. The percentage of events reported only by the ANF during each time period with respect to the total number of events reported is indicated in each panel.

and bin the events by 6 min intervals. Given that the seismicity rate in the central and eastern time zones is much lower than in the two western regions, events occurring within the two eastern regions are considered together.

Figure 9a shows the time-of-day distribution for all events occurring within the Pacific time zone. There are a few peaks of activity during local daytime hours (7 a.m.–7 p.m.), namely between 12 and 16 h. The observed rate of seismicity for weekend events is about constant, with only a slight increase visible at about 15.45 h. Figure 9b shows the local time distribution of events occurring within the Mountain time zone, with the stacked weekly seismicity rate level being roughly constant during the local night but increasing steadily to a peak around 16 h and decreasing as the day progresses. Larger peaks are seen at 12, 13, and 14 h. The stack of the weekend day's seismicity shows a similar pattern. The distribution of weekly seismicity in the central and eastern time zones is shown in Figure 9c. The rate of seismicity is much lower than in the Pacific and Mountain regions, note that vertical axis in Figure 9c is half of those in Figures 9a and b. The distribution of the rate of seismicity for these two regions is similar to that of the Pacific time zone with peaks in the rate of seismicity during daytime hours, namely between 11 and 18 h local time. For each of the above time zones, the rate of seismicity during local night hours is about constant as shown in Figure 9.

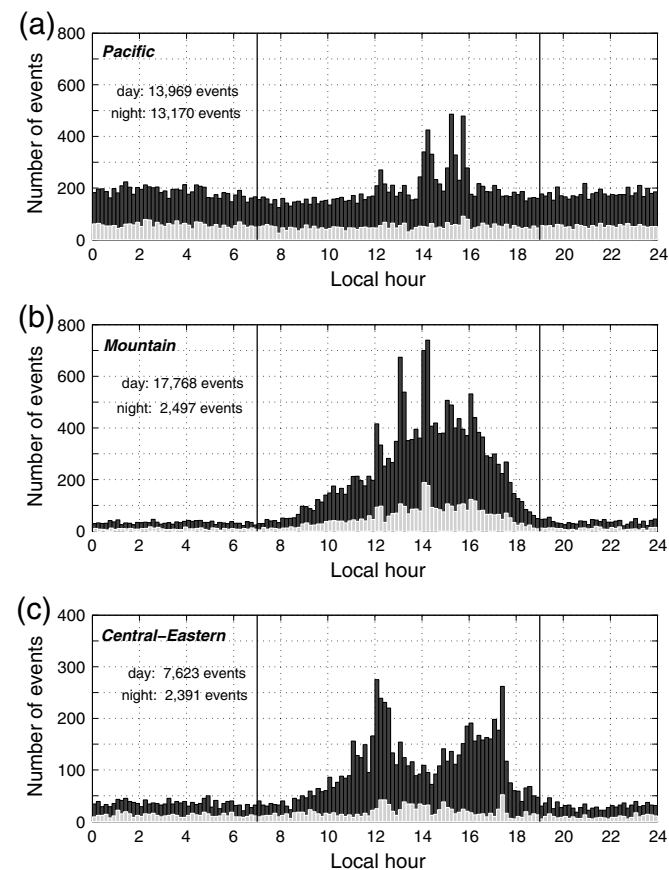
The rate of seismicity in the Pacific region is about six times greater than in other regions during local nighttime (Fig. 9), reflecting the higher tectonic stresses arising from the interaction of the Pacific and North America plates there. During local daytime hours, the seismicity rate in the Pacific region is only 6% higher, whereas in the other three regions it is

**Table 2**  
**Number of Events in the ANF Seismic Bulletin**

Time Period	Preferred Origins	Unique ANF Origins	Unique ANF/Preferred Origins (%)
April–December 2004	1861	37	2
2005	4353	217	5
2006	7724	2321	30
2007	10,117	5089	50
2008	7622	4797	63
2009	6769	5897	87
2010	5600	3996	71
2011	4796	2658	55
2012	4193	2462	59
January–November 2013	4569	3163	69
April 2004–November 2013	57,606	30,637	53.2

much higher, ranging from ~200% greater in the central United States to 700% greater in the Mountain time zone and 1500% greater in the eastern region.

The regulations of the Office of Surface Mining Reclamation and Enforcement (OSM) state that: “All blasting shall be conducted between sunrise and sunset, unless nighttime blasting is approved by the regulatory authority based upon a showing by the operator that the public will be protected from adverse noise and other impacts.” It is likely that the 18,058 events that occurred between April 2004 and November 2013 during local night hours show the natural seismicity in the contiguous United States. Hereafter, we follow the nomenclature for the physiographic regions defined by the USGS, following Fenneman and Johnson (1946) and Thelin and Pike (1991) (<http://tapestry.usgs.gov/physiogr/physio.html>; last accessed



**▲ Figure 9.** Comparisons of the overall week versus the weekend seismicity referred to local time in the continental United States. The dark bars show the result of stacking in 10 min intervals all events in a particular region as if they had occurred over a virtual day. The resulting distribution for events occurring only on weekend days is shown by the light gray histograms. Each graph shows results for events in different time zones: (a) Pacific, (b) Mountain, and (c) Central and Eastern. The number of events in each region during local night and day hours are indicated. The vertical lines show assumed local night/day boundary at 7 a.m., and the 7 p.m. day/night boundary.

March 2014). Figure 10 helps visualize the areal distribution of local day/nighttime seismicity in the continental United States where the local nighttime seismicity shown by blue circles overlays the location of events occurred during local daytime shown by the orange squares. Regions where mine blasting is the dominant source of seismic activity are readily apparent as local daytime events are not covered by nighttime seismicity.

Most of the local nighttime seismicity (18,058 events) in Figure 10 is located west of the 110° W meridian. This delineates the Pacific–North America plate boundary along the San Andreas fault system, the Pacific–Juan de Fuca plate boundary along the Mendocino and Blanco fracture zones in the Pacific Northwest, and deeper seismicity between the Juan de Fuca and North America plates in the Puget sound region. Crustal seismicity is well defined along the eastern boundary of the Sierra Nevada, the western boundary of the Basin and Range region in Nevada, the eastern boundary with the Colorado Plateau. Further north, seismicity occurs along the eastern boundary of the northern Rocky Mountains and the region surrounding Snake River Plain. East of the 110° W meridian, seismicity is more diffused and has gone mostly unreported (see Figs. 7 and 8). However, it is not clear if the seismicity recorded during the TA deployment was related to increased detection levels or to initiation of induced seismic activity due to natural gas exploitation in the region such as in Oklahoma in the Osage Plains (Holland and Gibson, 2012), or in Arkansas in the eastern boundary of the Ozark Plateaus and Ouachita province (Ellsworth, 2013). Doser *et al.* (1992) and Frohlich *et al.* (2011, 2012) have reported that seismicity recorded near the western boundary of the Coast Plain region in Texas may also be related to oil/gas production. A detailed discussion of induced seismicity is beyond the scope of this study, but has created great interest recently (Ellsworth, 2013; van der Elst *et al.*, 2013).

Although the location of the 39,360 local daytime events reported in the ANF Bulletin between April 2004 and November 2013 shows activity in similar regions as described in the previous paragraph, some event clusters of activity show mostly red squares. Included are those within the boundaries of British Columbia and Alberta, and in eastern Wyoming, where large surface coal mining operations are located. In northeastern Minnesota, the observed seismicity coincides with the location of surface iron mines. Higher seismicity is observed in the Appalachian region where underground coal mining is plentiful. Spatial mineral resource data is available through the USGS (<http://mrdata.usgs.gov/mineral-resources/mrds-us.html>; last accessed March 2014); a comprehensive database of all active and nonactive mines in the United States is available from the Mine Safety and Health Administration (<http://www.msha.gov/OpenGovernmentData/OGIMSHA.asp>; last accessed March 2014), which is a department of the U.S. Department of Labor. A list for Canadian mining operations is available from the Natural Resources Canada (<http://mmsd.mms.nrcan.gc.ca/stat-stat/mine-mine/index-eng.aspx>; last accessed April 2013). Figure 11 shows the location of active mines

in the states of conterminous United States and the southern-most Canadian provinces at the end of 2012.

Many large coal mines are located in eastern Wyoming and in the Appalachian Mountains. Both regions have low natural seismicity that makes them good candidates to investigate if most of ANF Seismic Bulletin events reported there are mine blasts, but a detailed analysis is beyond the scope of this study. The largest open-pit coal mining operations are found in eastern Wyoming, the events occurring in this region accounts for  $\sim 48\%$  of the total number of events occurred during daytime hours in the Mountain time zone (Fig. 9b). However, there are a handful of events occurring during the night (blue circles) in this region (see Fig. 10) that may have a tectonic origin. Regional seismic network operators are aware that daytime events occurring near-active mines are probably related to blasting in mines, (e.g., <http://earthquake.usgs.gov/earthquakes/eqarchives/mineblast/evidence.php>; last accessed March 2014). We have no explanation of the occurrence of some daytime seismicity occurring in regions such as western Tennessee (Fig. 10) where no active mines are located according to MSHA records (Fig. 11).

### Event Locations in the ANF Bulletin

The quality of the ANF Seismic Bulletin origins within the continental United States is given by the standard deviation of the travel-time residuals of the hypocentral solution (*slobs* in the CSS *origerr* table). Although this parameter does not provide a formal assessment of the location errors, we use it as a proxy to ascertain if the change in operational parameters had an effect on the overall event locations. The changes made in the automatic processing at ANF from  $na = 5$ , at the onset of the TA deployment (medium gray bars), to  $na = 10$  (dark gray bars) as the first USArray footprint was deployed (Fig. 1a), to the most recent change to  $na = 7$  (light gray bars) as USArray stations were being deployed in the central and eastern regions of the United States, gives us the opportunity to explore whether these operational changes have had an effect on event location quality. Figure 12 displays the distribution of *slobs* with different gray tones corresponding to the operational periods listed in  $\textcircled{E}$  Table S3. The number of events for the first operational period is largest for the Pacific zone, the largest number of events for the second period were located in the Mountain zone and those for the latter period in the central and eastern time zones.

The mean and median *slobs* values for each of the operational periods and the four time zone regions are listed in  $\textcircled{E}$  Table S3, with larger than 0.6 s mean *slobs* values occurring within each of the time zones at times when USArray stations did not provide good azimuthal coverage. Particularly, in the Pacific Time zone many events were located offshore, and the travel-time residuals of the hypocentral solutions tend to be larger as the IASPEI model is probably inappropriate for a region with rapid changes from oceanic to continental crust. Median *slobs* values for most regions listed in  $\textcircled{E}$  Table S3 are  $< 0.6$  s, with the exception of the most recent Mountain time zone events for which station coverage is sparse (Fig. 1d). The

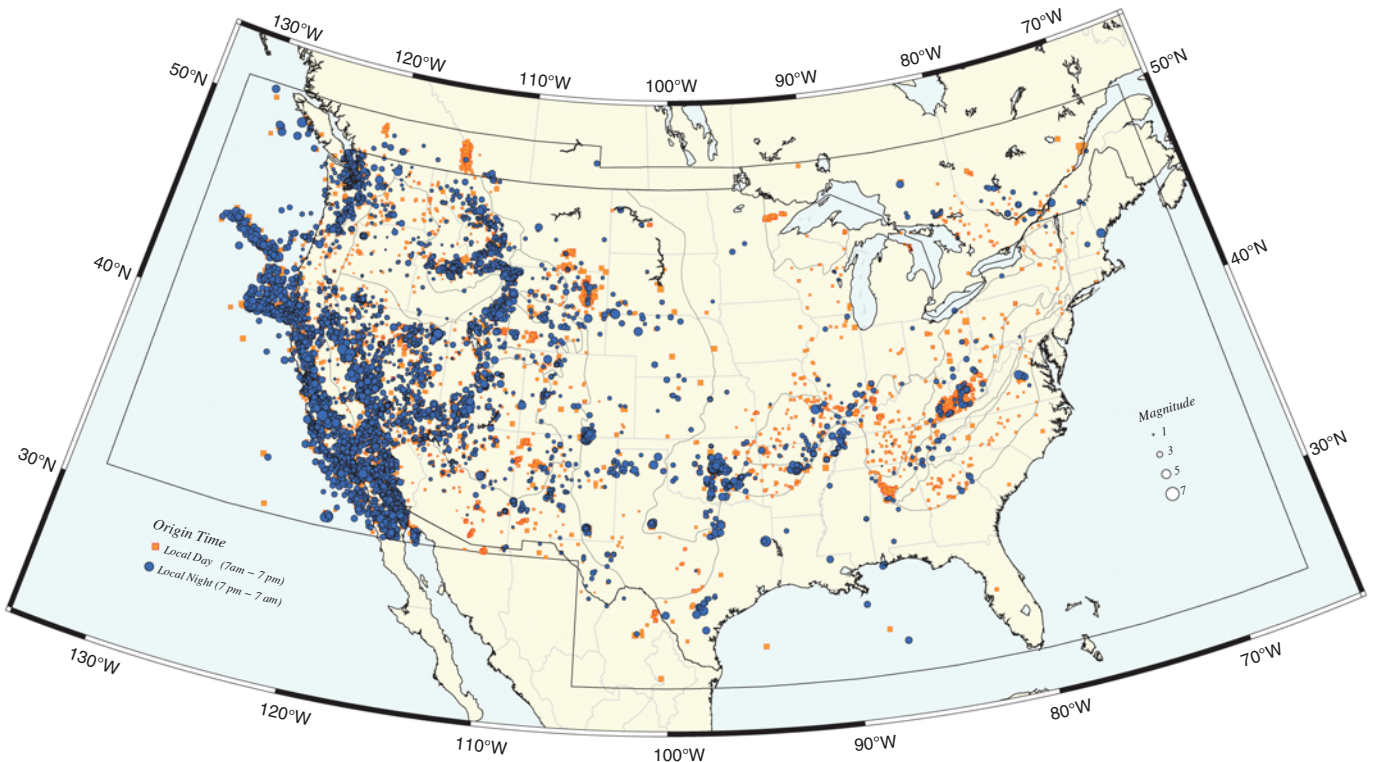
mean and median *slobs* value for events located by ANF between April 2004 and November 2013 is 0.53 and 0.47 s, respectively.

### Event Magnitudes in the ANF Bulletin

For the sake of uniformity and to account for the dynamic nature of the USArray, ANF computes magnitudes as defined by Richter (1958, pp. 340–344), which uses recordings of stations to distances of 600 km. To determine the magnitude threshold of the USArray as defined by the ANF Seismic Bulletin, we plot the total number of events with ANF origins in 0.1 magnitude increments in Figure 13. The bars and lines in all graphs in this figure show the  $M_R$  distribution for events occurring between April 2004 and November 2013. To determine if the operational changes carried out at the ANF affected the detection threshold in the ANF Seismic Bulletin, we divide the data into three groups corresponding to the time periods listed in  $\textcircled{E}$  Table S3. The distribution of the number of events occurring before and after 15 August 2007 are in medium and dark gray, respectively, in Figure 13a, with the light gray bars corresponding to the distribution of events occurring after 31 March 2012. The figure shows that there was a magnitude threshold, of about 1.8, corresponding to  $na = 5$  (minimum number of arrivals to trigger an event location) with higher thresholds for other periods. The inset displays the same information on a semilogarithmic scale, from which we can see that the negative slope of the three data groups is similar and parallel to that determined for all events, shown by the dark gray dashed line.

Figure 13b shows the magnitude distribution of events according its origin time referred local time. The dark histogram shows the magnitude distribution for those events occurring during local nighttime hours (blue circles in Fig. 10), with the medium gray histogram corresponding to the magnitude distribution of events occurring during local day hours (orange squares in Fig. 10). The detection threshold of events occurring at night is about 1.9 in contrast to the higher magnitude detection level of about 2.3 for daytime events. The number of events with  $M_R \geq 4.0$  is about the same for both day and nighttime groups. The MSHA limits the size of mining blasts to prevent accidents, which explains the increase in smaller magnitude events during daytime hours as shown in the inset in Figure 13b, in which it is clear that the slope of the daytime line is steeper for smaller sized events. Levels of lower cultural noise may explain the lower detection threshold, thus leading to and increased capability of the USArray to detect smaller earthquakes.

The largest discrepancy in the number of events occurring between day and night was observed for the Mountain and eastern zones. We plot the magnitude distribution of events occurring in the Pacific, Mountain, central and eastern time zones according to the epicenter's local time. Figure 14 shows the magnitude distribution of Pacific time zone events, for which both day and night distributions are similar, with an increase of events with  $M_R < 3.0$  during local daytime. The distribution for the other three groups shows an increase in

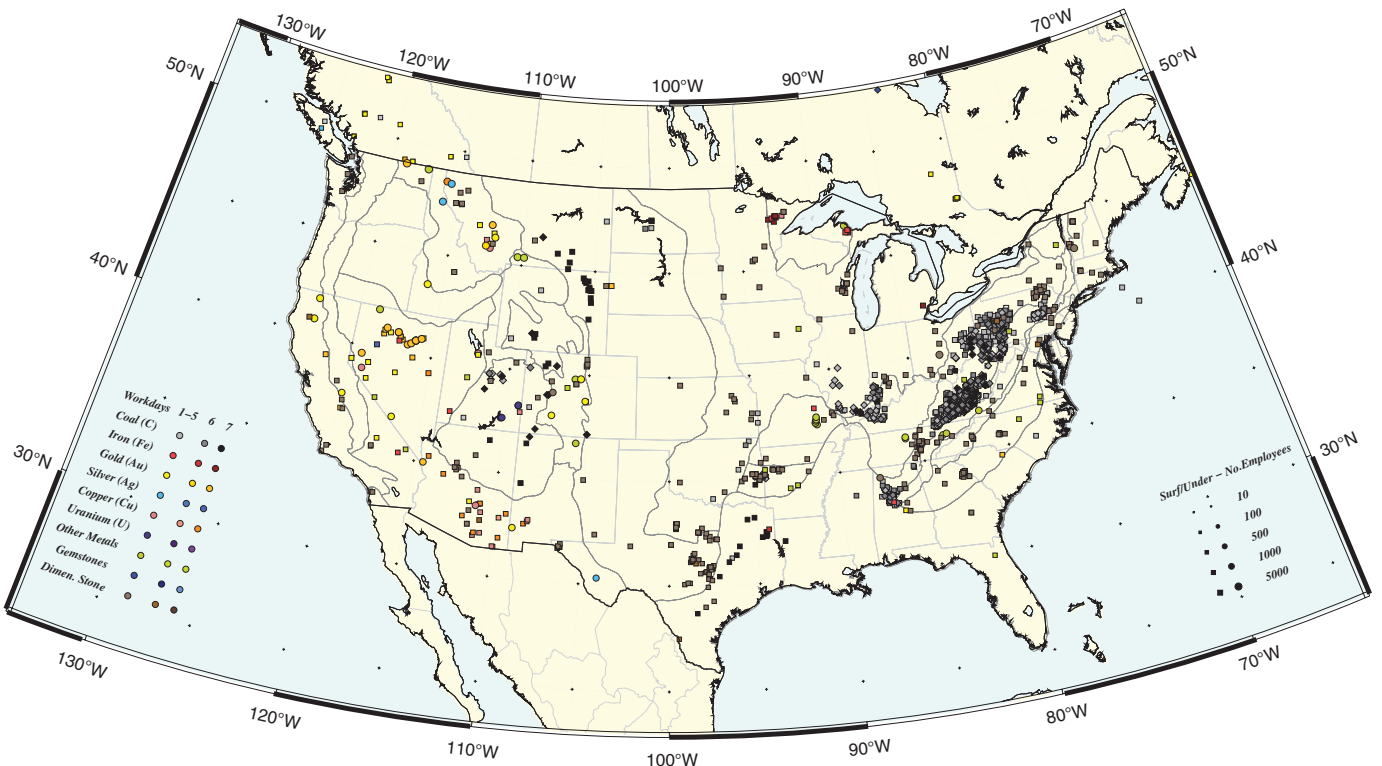


**▲ Figure 10.** Comparison of local day/night hour seismicity as reported in the ANF Seismic Bulletin between April 2004 and November 2013. Events occurring during local daytime hours are plotted with red squares, and those occurring during local night time with blue circles. Symbol size is proportional to magnitude. Light gray lines show political boundaries and dark lines the physiographic regions as defined by the USGS (<http://tapestry.usgs.gov/physiogr/physio.html>; last accessed March 2014).

$M_R < 4.0$  events in the Mountain region, for  $M_R < 3.0$  events in the central and for all magnitudes in the eastern region (Fig. 14). However, the August 2011 Virginia earthquake occurred during the day. The difference in the largest magnitude of additional events (from 4 to 3) occurring during daytime hours in the Mountain and central time zones suggest that in sparsely populated areas of states such as Wyoming, Montana, Utah, and Nevada (where larger mining operations exist) more energetic blasts may be allowed. The magnitude distribution of ANF Bulletin events occurring during local night hours is similar for all regions, as indicated by the red dashed line in each of the lower panels in Figure 14. By considering the seismicity occurring during local night only for each region, the magnitude threshold for the Pacific and Mountain regions is  $M_R \sim 1.8$ , whereas for the central regions is  $M_R \sim 2.1$  as shown in Figure 14. The magnitude threshold for nighttime events in the eastern zone is hard to assess but for those occurring during the day is about 2.4 similar to daytime seismicity occurring in the central time zone. The daytime threshold for the Pacific and Mountain zones is lower,  $M \sim 2.0$  and  $\sim 2.2$ , respectively.

Regional network operators in the United States routinely determine magnitudes for events occurring within their monitoring area. These determinations are collected and associated with the corresponding event by seismic analysts at the ANF.

Network operator abbreviations used hereafter and in the author field within the CSS tables at ANF are included (E) Table S3. The Southern California Seismic Network (SCSN) still estimates magnitudes as defined by Richter in 1958 (E. Hauksson, personal comm., 2013) and reports it as local magnitude ( $M_L$ ). However, other regional network operators report local magnitude for events, which has been modified empirically from the original  $M_R$  definition to account for site conditions as well as the distribution of stations comprising each regional network (e.g. Pechmann, *et al.*, 2007). Given the layout of the USArray, many more stations at larger distances are included to determine  $M_R$ , a fact that can bias ANF's magnitude determinations upward for events in the central and eastern regions of the United States because attenuation is smaller than in the western United States (e.g. Chapman *et al.*, 2008, Atkinson, 2004). For emphasis, we plot the difference with respect to  $M_R = M_L$  for the relationship of  $M_R$  determined at ANF with local magnitudes ( $M_L$ ) and moment magnitude ( $M_w$ ) in Figure 15a and b, respectively, as reported by regional seismic catalogs. The relationships are defined by the least-square line fit to the data shown in (E) Figures S6 and S7, respectively. The width of the lines is proportional to the number of events and the colors correspond to those used in Figure 7. Not surprisingly, the difference for the  $M_R - M_L$  relationship for southern California



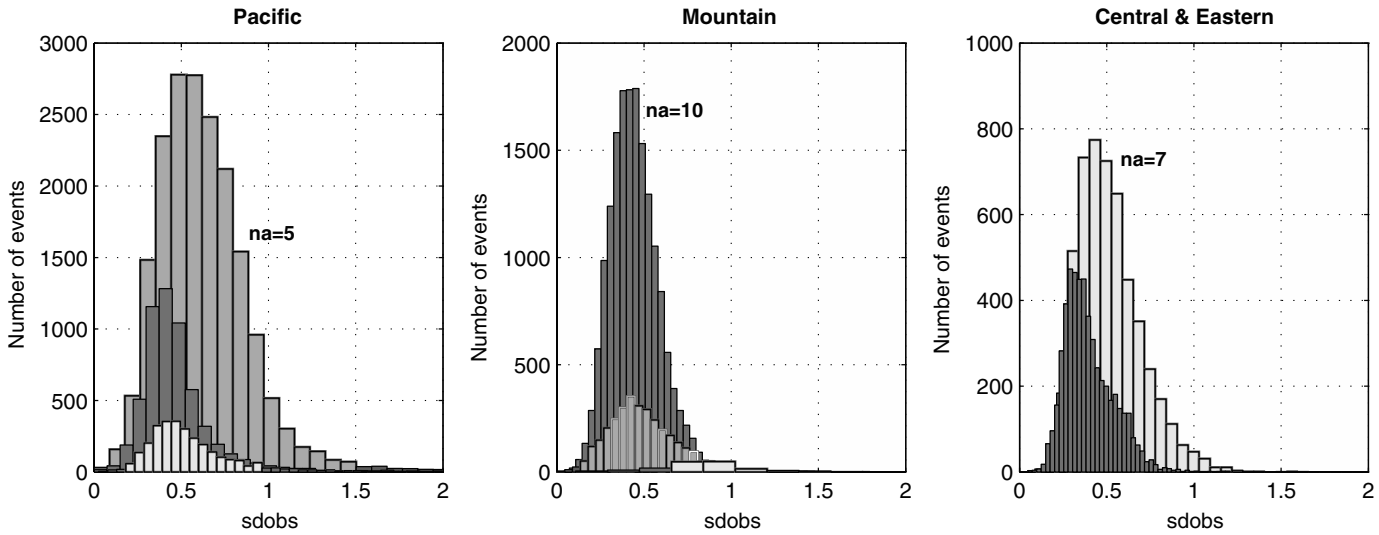
**▲ Figure 11.** Location of active mines in the contiguous United States and the southernmost Canadian provinces (U.S.: <http://www.msha.gov/OpenGovernmentData/OGIMSHA.asp>; last accessed March 2014). The symbol sizes are proportional to the number of people who work at each mine. The legend to the left shows the mineral that is being extracted at each mine with the color intensity varying according to the number of weekly work days for each mine.

events is almost one-to-one, (shown by the thick orange line). The slope of the least-squares-fit line to the data amongst these operators varies from 0.8 for northern California events as reported by Northern California Seismic Network (NCSN) and for events occurred in Utah and Yellowstone as reported by Utah University Seismic Service (UUSS) and shown in (E) Figure S6a. A slope of 0.7 was estimated for events occurring in the Pacific Northwest (both in Canada, Pacific Geoscience Center and the United States, Pacific Northwest Seismic Network [PNSN], (E) Fig. S6a) as well as events occurring in Nevada as reported by Nevada Bulletin of Earthquakes-University of Nevada at Reno (UNR-NBE), and Montana as reported by Montana Tech of the University of Montana (MTECH) (E) Fig. S6a).

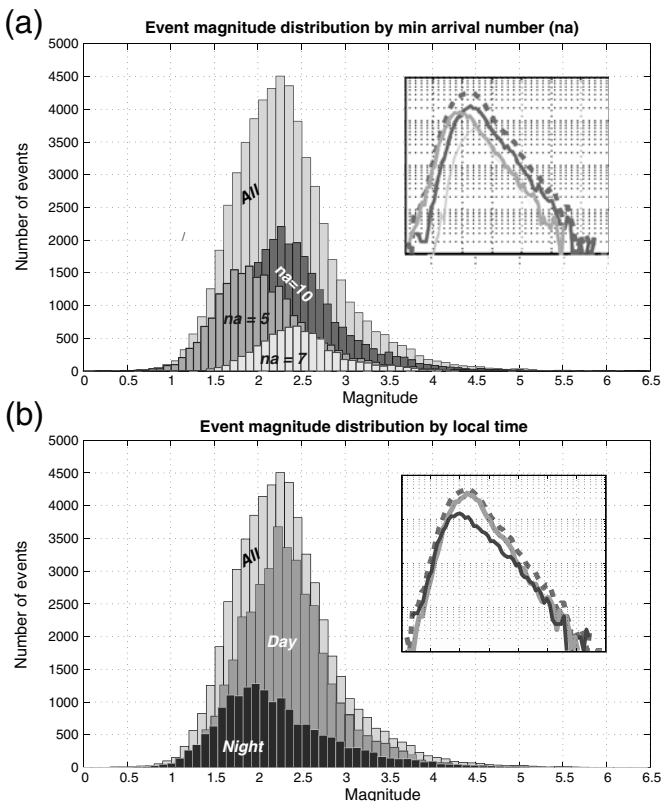
The relationship of  $M_R$  determined by ANF to magnitudes of events reported by seismic networks in the central and eastern United States is shown in (E) Figure S6b. The top panels show the relationship of  $M_R$  to that of  $M_L$  determined at Center of Earthquake Research Institute (CERI) for events occurring in the New Madrid region and for events occurring in the northeastern United States as reported by Lamont-Doherty Columbia Seismic Network, which show slopes of 0.6 and 0.5, respectively). The lower panels show the relationship of  $M_R$  calculated at ANF to other magnitudes determined by

regional network operators in the central and eastern United States such as  $m_{blg}$  reported for a few events by CERI (E) middle panels Fig. S6b) and the GSC as well as  $m_c$  (coda magnitude) reported by the Northeast Seismic Network (E) lower panel in Fig. S6b). The difference of the relationship of ANF's  $M_R \sim 3.0$  vary by 0.5 magnitude, for larger magnitudes, for example,  $M_R \sim 5.0$  the variation with respect to other magnitudes expands to about 1.2 for magnitudes reported in western, central, and eastern United States seismic catalogs. This occurs because magnitudes estimated at ANF use more stations at further distances which have larger amplitudes due to lesser attenuation in this region (e.g., McNamara, *et al.*, 2014), increasing the value of  $M_R$  with respect to stations in southern California where  $M_R$  was defined (Richter, 1958).

The differences shown for the relationship of  $M_R$  determined by ANF with respect to  $M_w$  determined by seismic networks in the northern California and Mountain regions (E) Fig. S7) show a similar distribution as those observed for  $M_L$  relationships. However, the relationship of  $M_w$  reported by the SCSN network suggest that  $M_L$  magnitudes as defined by Richter would tend to give larger magnitude values if many stations at larger ranges were included in the calculation as is the case with  $M_R$  determined at ANF. Although, it would be possible to assess the variation of mag-



▲ **Figure 12.** Histograms showing the distribution of the location misfit of ANF origins (*sdobs*) grouped by the local time zone in which events occurred. Medium gray bars correspond to events that occurred before 16 August, 2007, dark gray bars to those events occurred between 15 August, 2007, and 1 April 2012 and light gray bars show the distribution for events occurring after 31 March 2012.

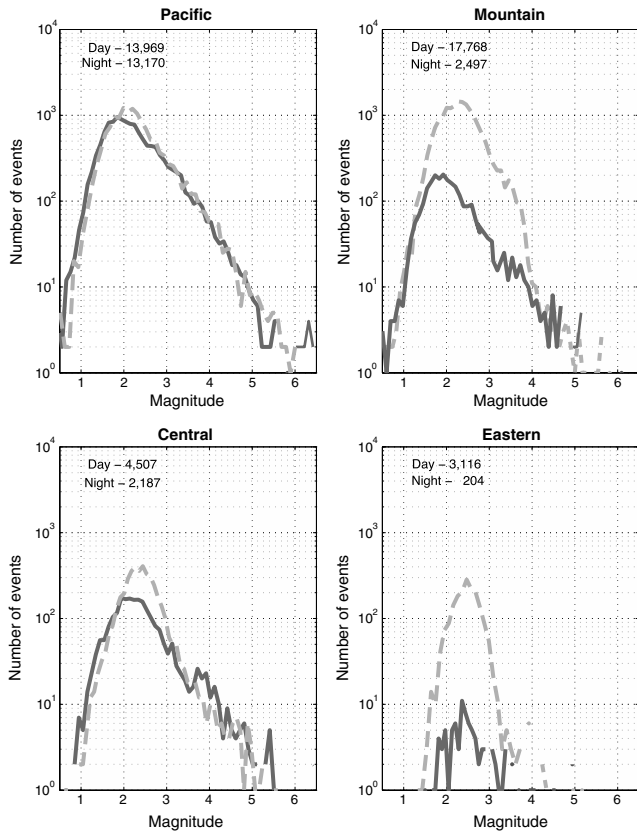


▲ **Figure 13.** Event magnitude ( $M_R$ ) distribution by (a) minimum number of arrivals (*na*) required for triggering an event location. (b) Event magnitude ( $M_R$ ) distribution of events occurring during local day hours (7 a.m.–7 p.m.) and night hours (7 p.m.–7 a.m.). Bin size is 0.1 unit magnitude in both all graphs. The insets in both panels show the same information in a semilogarithmic scale.

nitude with distance as the ANF Bulletin includes individual station magnitudes for each event to try to determine a rough variation of attenuation across the United States, it is beyond the scope of this study. For completeness, graphs showing the relationship of  $M_R$  as determined by ANF to duration magnitude ( $M_d$ ) as reported by PNSN, NCSN, UNR-NBE, MTECH, UUSS, and CERI (Fig. S8).

## CONCLUSIONS

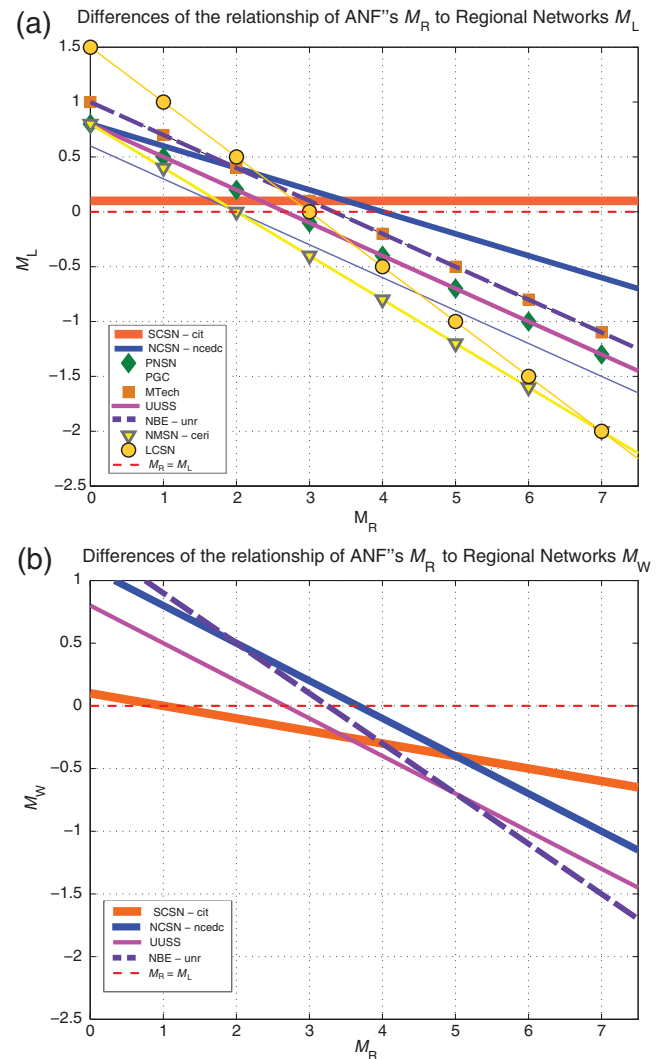
As of 30 November 2013, the ANF Seismic Bulletin included over 6.7 million phase picks associated with about 78,000 events recorded at USAArray stations. Arrivals for earthquakes with  $M \geq 5.0$  occurring worldwide comprise the bulk of arrivals reported in the bulletin, as most stations within the deployment record seismic waves produced by these events. ANF analysts associate these arrivals to hypocentral locations reported by the NEIC seismic catalog. Events occurring within the continental United States comprises the bulk of the ANF Bulletin (57,606) being located first automatically in quasi-real time and then are reviewed by ANF analysts using the IASP91 velocity model. The mean and median standard deviation travel-time residuals for these locations are 0.53 and 0.48 s, respectively. If regional network operators report a location for a particular event, the arrivals are associated and that origin deemed authoritative if the event is located within a particular network region. The ANF Bulletin is comprehensive, as it does not attempt to distinguish between natural and anthropogenic seismic sources, resulting in the ANF Bulletin reporting about double the number events for the same time period than other regional seismic networks. Figure 16 shows the distribution of the number of events in 6 min bins referred to local time of all events recorded between April 2004 and November 2013 by



**▲ Figure 14.** Comparison of the magnitude distribution of events occurring during the night (dark continuous lines) and day (dashed light gray lines) for the Pacific, Mountain, central, and eastern time zones. The number of events that occurred in each region during local day and nighttime hours are indicated in each panel.

USArray in the contiguous United States as if they had occurred on a single virtual day. In this graph, the red dashed line shows the background seismicity level, as viewed by USArray, indicating that approximately 36,000 events in the ANF Bulletin are tectonic in origin, and about 20,000 events are not. The peaks in seismic activity just after 11, 12, 13, 14, 15, and 17 h are further evidence that these events are connected to human activity. A movie of the seismic activity referred to local time of all events occurring between April 2004 and November 2013 in the continental United States as if occurred within a virtual day is included in **④ Movie S3**. Clusters of seismic activity occurring during local day hours and apparent at the times listed above are situated near active mines (Fig. 11). However, even if those 20,000 events had been caused by mine blasts, ANF analysts have located an additional 9000 events. This suggests that the ANF Bulletin has located many more tectonic events than those reported for the same period by regional seismic networks.

$M_R$  has been calculated for most events occurring within the contiguous United States, we estimate that the detection threshold for USArray is approximately 2.3 overall and about 1.9 for events occurring during the night as cultural noise is lower at those times. As the TA component of the USArray

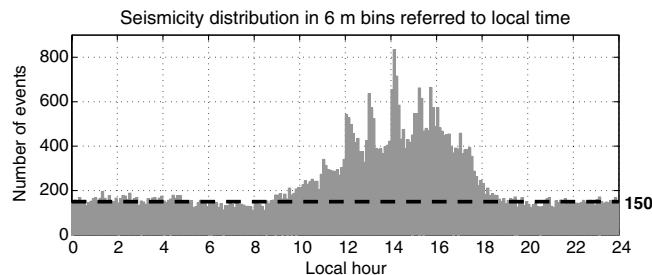


**▲ Figure 15.** Difference with respect to  $M_R = M_L$  for the relationships between  $M_R$  reported in the ANF Bulletin and local magnitude, (a)  $M_L$  and (b)  $M_W$  as reported by regional seismic networks (Table 1). The relationships are defined by the least square line fit to the data shown in **④ Figures S6 and S7**, respectively. The width of the lines is proportional to the number of events, and the colors correspond those used in Figure 7.

continues its deployment further east, the ANF will continue to perform its tasks completing the arrival data set for teleseismic and regional events located in the array footprint by the summer of 2015 when most TA stations will be decommissioned as the EarthScope USArray project ends.

## DATA AND RESOURCES

The array network facility (ANF) Seismic Bulletin CSS3.0 tables are available at <http://anf.ucsd.edu/tools/events/download.php> (last accessed March 2014). USArray transportable array (TA) metadata is available at <http://anf.ucsd.edu/tools/dataless/> (last



▲ **Figure 16.** Stack of overall seismicity in the continental United States referred to local time in 6 min intervals. The dashed horizontal line shows the background seismicity level for events occurring between April 2004 and November 2013 in the contiguous United States.

accessed March 2014) and other ancillary information about USArray stations is available at <http://anf.ucsd.edu> (last accessed March 2014). The software used is described in the text of the article. Maps and plots were generated using the Generic Mapping Tool (GMT; Wessel and Smith, 1998; <http://gmt.soest.hawaii.edu/>; last accessed November 2012). □

## ACKNOWLEDGMENTS

We thank the Mining Safety and Health Administration (MSHA) staff, in particular, William West and Chad Hancher, for pointing us to the correct link to access the active mines database in their website. Editorial comments to an earlier version and discussion with Carl Ebeling and Peter Shearer greatly improved this manuscript, as did the comments and suggestions of Zhigang Peng, SRL Editor, and an anonymous reviewer. We use GMT (Wessel and Smith, 1991, 1995a,b, 1998) to produce most figures in this manuscript. This material is based upon work supported by the Incorporated Research Institutions for Seismology under their Cooperative Agreement Number EAR-0733069 with the National Science Foundation.

## REFERENCES

- Agnew, D. C. (1990). The use of time-of-day seismicity maps for earthquake/explosion discrimination by local networks, with an application to the seismicity of San Diego County, *Bull. Seismol. Soc. Am.* **80**, 747–750.
- Astiz, L., P. Earle, and P. Shearer (1996). Global stacking of broadband seismograms, *Seismol. Res. Lett.* **67**, 8–18.
- Atkinson, G. M. (2004). Empirical attenuation of ground-motion spectral amplitudes in southeastern Canada and the northeastern United States, *Bull. Seismol. Soc. Am.* **94**, 1079–1095.
- Bratt, S. R., and T. C. Bache (1988). Locating events with a sparse network of regional arrays, *Bull. Seismol. Soc. Am.* **78**, 780–798.
- Buehler, J. S., and P. M. Shearer (2010). *Pn* tomography of the western United States using USArray, *J. Geophys. Res.* **115**, no. B009315, 12 pp., doi: [10.1029/2009JB006874](https://doi.org/10.1029/2009JB006874).
- Burdick, S., Ch. Li, V. Martynov, T. Cox, J. Eakins, T. Mulder, L. Astiz, F. L. Vernon, G. L. Pavlis, and R. D. van der Hilst (2008). Upper mantle heterogeneity beneath North America from travel time tomography with global and USArray Transportable Array data, *Seismol. Res. Lett.* **79**, no. 3, 384–392, doi: [10.1785/gssrl.79.3.384](https://doi.org/10.1785/gssrl.79.3.384).
- Burdick, S., R. D. van der Hilst, F. L. Vernon, V. Martynov, T. Cox, J. Eakins, T. Mulder, L. Astiz, and G. L. Pavlis (2009). Model update December 2008: Upper mantle heterogeneity beneath North America from P-wave travel time tomography with global and USArray Transportable Array data, *Seismol. Res. Lett.* **80**, no. 4, 638–645, doi: [10.1785/gssrl.80.4.638](https://doi.org/10.1785/gssrl.80.4.638).
- Burdick, S., R. D. van der Hilst, F. L. Vernon, V. Martynov, T. Cox, J. Eakins, G. H. Karasu, J. Tytell, L. Astiz, and G. L. Pavlis (2010). Model update January 2010: Upper mantle heterogeneity beneath North America from P-wave traveltimes tomography with global and USArray Transportable Array data, *Seismol. Res. Lett.* **81**, no. 5, 689–693, doi: [10.1785/gssrl.81.5.689](https://doi.org/10.1785/gssrl.81.5.689).
- Burdick, S., R. D. van der Hilst, F. L. Vernon, V. M. Martynov, T. Cox, J. Eakins, G. H. Karasu, J. Tytell, L. Astiz, and G. L. Pavlis (2012). Model update March 2011: Upper mantle heterogeneity beneath North America from traveltimes tomography with global and USArray Transportable Array data, *Seismol. Res. Lett.* **83**, no. 1, 23–28, doi: [10.1785/gssrl.83.1.23](https://doi.org/10.1785/gssrl.83.1.23).
- Burdick, S., R. D. van der Hilst, F. L. Vernon, V. M. Martynov, T. Cox, J. Eakins, G. H. Karasu, J. Tytell, L. Astiz, and G. L. Pavlis (2013). Model Update January 2013: Upper Mantle Heterogeneity beneath North America from Traveltimes Tomography with Global and USArray Transportable Array Data, *Seismol. Res. Lett.* **85**, no. 1, 77–81, doi: [10.1785/02220130098](https://doi.org/10.1785/02220130098).
- Chapman, M. C., J. N. Beale, and R. D. Catchings (2008). *Q* for *P* waves in the sediments of the Virginia coastal plain, *Bull. Seismol. Soc. Am.* **98**, 2022–2032, doi: [10.1785/0120070170](https://doi.org/10.1785/0120070170).
- Doser, D. I., M. R. Baker, M. Luo, P. Marroquin, L. Ballesteros, J. Kingwell, H. L. Diaz, and G. Kaip (1992). The not so simple relationship between seismicity and oil production in the Permian basin, West Texas, *Pure Appl. Geophys.* **139**, no. 3/4, 481–506.
- Ellsworth, W. L. (2013). Injection-induced earthquakes, *Science* **341**, no. 6142, doi: [10.1126/science.1225942](https://doi.org/10.1126/science.1225942).
- Fenneman, N. M., and D. W. Johnson (1946). Physical divisions of the United States, *U.S. Geol. Surv.*, scale 1:7,000,000.
- Ford, S. R., D. S. Dreger, and W. R. Walter (2008). Source characterization of the 6 August 2007 Crandall Canyon mine seismic event in central Utah, *Seismol. Res. Lett.* **79**, 637–644, doi: [10.1785/gssrl.79.5.637](https://doi.org/10.1785/gssrl.79.5.637).
- Frohlich, C., C. Hayward, B. Stump, and E. Potter (2011). The Dallas–Fort Worth earthquake sequence: October 2008 through May 2009, *Bull. Seismol. Soc. Am.* **101**, 327–340, doi: [10.1785/0120100131](https://doi.org/10.1785/0120100131).
- Frohlich, C., J. Glidewell, and M. Brunt (2012). Location and felt reports for the 25 April 2010  $m_{bLg}$  3.9 earthquake near Alice, Texas: Was it induced by petroleum production, *Bull. Seismol. Soc. Am.* **102**, 457–466, doi: [10.1785/0120110179](https://doi.org/10.1785/0120110179).
- Holland, A. A., and A. R. Gibson (2012). Analysis of the Jones, Oklahoma earthquake swarm, *Seismol. Res. Lett.* **82**, 327.
- Holland, A. A., A. R. Gibson, C. Chen, G. R. Keller, and K. V. Luza (2012). Incorporating near real-time transportable array data in the regional Oklahoma seismic network, *Seismol. Res. Lett.* **82**, 358.
- Kanamori, H. (1983). Magnitude scale and quantification of earthquakes, *Tectonophysics* **93**, 185–199.
- Kennett, B. (1991). *LASPEI 1991 Seismological Tables*, Bibliothech, Canberra, Australia, 167 pp.
- Kennett, B., and E. R. Engdahl (1991). Traveltimes for global earthquake location and phase identification, *Geophys. J. Int.* **105**, 429–465.
- Lockridge, J. S., M. J. Fouch, and J. R. Arrowsmith (2012). Seismicity within Arizona during the deployment of the EarthScope USArray Transportable Array, *Bull. Seismol. Soc. Am.* **102**, doi: [10.1785/0120110297](https://doi.org/10.1785/0120110297).
- McNamara, D., L. Gee, H. M. Benz, and M. Chapman (2014). Frequency-dependent seismic attenuation in the eastern United States as observed from the 2011 Central Virginia earthquake and after-

- shock sequence, *Bull. Seismol. Soc. Am.* **104**, 55–72, doi: [10.1785/0120130045](https://doi.org/10.1785/0120130045).
- Pavlis, G. L., F. Vernon, D. Harvey, and D. Quinlan (2004). The generalized earthquake-location (GENLOC) package: An earthquake-location library, *Comput. Geosci.* **30**, 1078–1091.
- Pechmann, J. C., S. J. Nava, F. M. Terra, and J. C. Bernier (2007). Local magnitude determinations for Intermountain Seismic Belt earthquakes from broadband digital data, *Bull. Seismol. Soc. Am.* **97**, 557–574.
- Pechmann, J. C., W. J. Arabasz, K. L. Panknow, R. Bulacu, and M. McCarter (2008). Seismological report on the 6 August 2007 Crandall Canyon mine collapse in Utah, *Seismol. Res. Lett.* **79**, 620–636, doi: [10.1785/gssrl.79.5.620](https://doi.org/10.1785/gssrl.79.5.620).
- Richter, C. F. (1958). *Elementary Seismology*, First Ed., W.H. Freeman and Company, San Francisco, U.S.A., 768 pp.
- Thelin, G. P., and R. J. Pike (1991). Landforms of the conterminous United States: A digital shaded-relief portrayal, *U.S. Geol. Surv. Map I-2206*.
- van der Elst, N. J., H. M. Savage, K. M. Keranen, and G. A. Abers (2013). Enhanced remote earthquake triggering at fluid-injections sites in the Midwest United States, *Science* **341**, 164–167, doi: [10.1126/science.1238948](https://doi.org/10.1126/science.1238948).
- Wessel, P., and W. H. F. Smith (1991). Free software helps map and display data, *Eos Trans. AGU* **72**, no. 41, 441, 445–446.
- Wessel, P., and W. H. F. Smith (1995a). New version of the Generic Mapping Tools released, *Eos Trans. AGU* **76**, no. 33, 329.
- Wessel, P., and W. H. F. Smith (1995b). New version of the Generic Mapping Tools released, *Eos Trans. AGU*, electronic supplement, [http://www.agu.org/eos\\_elec/95154e.html](http://www.agu.org/eos_elec/95154e.html) (last accessed April 2013).
- Wessel, P., and W. H. F. Smith 1998 New, improved version of Generic Mapping Tools released, *Eos Trans. AGU* **79**, no. 47, 579.

*Luciana Astiz  
Jennifer A. Eakins*

*Vladislav G. Martynov  
Trilby A. Cox  
Jonathan Tytell  
Juan C. Reyes  
Robert L. Newman\*  
Gulsüm H. Karasu†  
Taimi Mulder‡  
Malcolm White  
Geoffrey A. Davis  
Jon C. Meyer  
Frank L. Vernon*

*Institute of Geophysics and Planetary Physics  
Scripps Institution of Oceanography  
University of California San Diego  
La Jolla, California 92093-0225 U.S.A.  
lastiz@ucsd.edu*

*Robert W. Busby  
Katrin Hafner  
Incorporated Research Institutions for Seismology  
Data Management Center  
1200 New York Avenue NW  
Washington, D.C. 20005 U.S.A.*

---

\* Now at Incorporated Research Institutions for Seismology Data Management Center, 1200 New York Avenue NW, Washington, D.C. 20005 U.S.A.

† Now retired.

‡ Now at Pacific Geoscience Centre, Sidney, British Columbia, Canada.